ATLAS NOTE

ATLAS-CONF-2012-103

August 10, 2012

Search for new phenomena using large jet multiplicities and missing transverse momentum with ATLAS in 5.8 fb^{-1} of $\sqrt{s}$ = 8 TeV proton-proton collisions

The ATLAS Collaboration

Abstract

A search is presented for new particles decaying to large numbers of jets in association with missing transverse momentum, using 5.8 fb^{-1} of pp collision data at $\sqrt{s}$ = 8 TeV collected by the ATLAS experiment at the Large Hadron Collider in 2012. The event selection requires missing transverse momentum, no isolated electrons or muons, and from ≥6 to ≥9 jets. No evidence is found for physics beyond the Standard Model. The results are interpreted in the context of a simplified supersymmetry model containing only a gluino octet and a neutralino, where pair-produced gluinos each decay into $t + \bar{t} + \tilde{\chi}_1^0$. In this context gluino masses smaller than 1.0 TeV are excluded at the 95% CL for neutralino masses below 300 GeV.

ATLAS-CONF-2012-103
13 August 2012

1 Introduction

Many extensions of the Standard Model of particle physics predict the presence of TeV-scale strongly interacting particles that decay to lighter, weakly interacting descendants. Any such weakly interacting particles that are massive and stable can contribute to the dark matter content of the universe. The strongly interacting parents would be produced in the proton-proton interactions at the Large Hadron Collider (LHC), and such events would be characterized by significant missing transverse momentum $E_{\mathrm{T}}^{\mathrm{miss}}$ from the unobserved weakly interacting daughters, and jets from emissions of quarks and/or gluons.

In the context of R-parity conserving supersymmetry (SUSY) [1] the strongly interacting parent particles are the squarks $\tilde{q}$ and gluinos $\tilde{g}$; they are produced in pairs, and the lightest supersymmetric particles can provide stable dark matter candidates [2]. Jets are produced from a variety of sources: from quark emission in supersymmetric cascade decays, production of heavy Standard Model particles (W, Z or t) which then decay hadronically, or from QCD radiation. Examples of particular phenomenological interest include models where squarks are significantly heavier than gluinos. In such models the gluino pair production and decay process

$$\tilde{g} + \tilde{g} \rightarrow \left(t + \bar{t} + \tilde{\chi}_1^0\right) + \left(t + \bar{t} + \tilde{\chi}_1^0\right) \tag{1}$$

can dominate, producing large jet multiplicities when the resulting top quarks decay hadronically.

Searches for new phenomena in final states with large jet multiplicities – requiring from at least six to at least nine jets – have previously been reported by the ATLAS [3] collaboration using LHC pp collision data corresponding to $1.34\,\mathrm{fb}^{-1}$ [4] and to $4.7\,\mathrm{fb}^{-1}$ [5] at $\sqrt{s} = 7$ TeV. Searches with explicit tagging of b-jets in multi-jet events were also performed [6]. In this note, we present an analysis of the pp collision data recorded by the ATLAS experiment during the period from March to June 2012 at a centre-of-mass energy of $\sqrt{s} = 8$ TeV and corresponding to integrated luminosity of approximately $5.8\,\mathrm{fb}^{-1}$. The increase of centre-of-mass energy from 7 TeV to 8 TeV leads to an increase in the cross-section for the process $pp \rightarrow \tilde{g}\tilde{g}$ by a factor of about 2.4 for gluino masses close to 1 TeV.

The search strategy follows closely that used at 7 TeV [5]. Events are selected with large jet multiplicities, with requirements ranging from at least six to at least nine jets, together with significant $E_{\mathrm{T}}^{\mathrm{miss}}$. Events containing isolated, high-p_{T} electrons or muons are vetoed in order to reduce backgrounds involving leptonic W boson decays.

2 The ATLAS detector and data samples

The ATLAS experiment [3] is a multi-purpose particle physics detector with a forward-backward symmetric cylindrical geometry and nearly 4π coverage in solid angle.[1] The layout of the detector is dominated by four superconducting magnet systems, which comprise a thin solenoid surrounding inner tracking detectors (ID), and a barrel and two end-cap toroids supporting a large muon spectrometer. The calorimeters are of particular importance to this analysis. In the pseudorapidity region $|\eta| < 3.2$, high-granularity liquid-argon (LAr) electromagnetic (EM) sampling calorimeters are used. An iron/scintillator-tile calorimeter provides hadronic coverage for $|\eta| < 1.7$. The end-cap and forward regions, spanning $1.5 < |\eta| < 4.9$, are instrumented with LAr calorimetry for both EM and hadronic measurements.

The data sample used in this analysis was taken during the period from March to June 2012 with the LHC operating at a proton-proton centre-of-mass energy of $\sqrt{s} = 8$ TeV. Application of beam, detector

[1] ATLAS uses a right-handed coordinate system with its origin at the nominal interaction point in the centre of the detector and the z-axis along the beam pipe. Cylindrical coordinates (r, ϕ) are used in the transverse plane, ϕ being the azimuthal angle around the beam pipe. The pseudorapidity η is defined in terms of the polar angle θ by $\eta = -\ln\tan(\theta/2)$.

and data-quality requirements resulted in a corresponding integrated luminosity of $5.8 \pm 0.2\,\text{fb}^{-1}$, where the luminosity is measured using similar techniques to those described in Ref. [7]. The analysis makes use of dedicated multi-jet triggers that required either at least five jets with $p_{\text{T}} > 55$ GeV or at least six jets with $p_{\text{T}} > 45$ GeV, where the jets must have $|\eta| < 3.2$. At the last stage of online trigger selection the jet algorithm and calibration method used are closely matched to those used in the offline selection. In all cases the trigger efficiency was greater than 98% for events satisfying the offline jet multiplicity selections described in Section 4.

3 Object Selection

Jet candidates are reconstructed using the anti-k_t jet clustering algorithm [8, 9] with radius parameter of 0.4. The inputs to this algorithm are clusters of calorimeter cells seeded by cells with energy significantly above the noise level. The local cluster weighting (LCW) calibration method [10, 11] classifies topological clusters as either being of electromagnetic or hadronic origin and based on this classification applies specific energy corrections derived from a combination of Monte Carlo simulation and data. This LCW provides an improved jet energy resolution compared to that used in Ref. [5]. The dependence of the jet response on pile-up is largely canceled by offset corrections derived as a function of the average number of interactions per event $\langle\mu\rangle$ and of the number of primary vertices N_{PV}. Except during $E_{\text{T}}^{\text{miss}}$ computation, two minimal requirements are made on jet acceptance: $p_{\text{T}} > 20$ GeV and $|\eta| < 2.8$.

Electron candidates are reconstructed from clusters of cells in the electromagnetic calorimeter matched to a track in the ID. They are required to have $p_{\text{T}} > 20$ GeV and $|\eta| < 2.47$, and to satisfy the electron shower shape and track selection criteria of Ref. [12], with modifications to reduce the impact of pile-up and cope with tighter trigger requirements induced by the higher instantaneous luminosity. Electrons are accepted if $E_{\text{T}} > 20$ GeV and $|\eta| < 2.47$ where $E_{\text{T}} = E^{\text{clust}}/\cosh\eta$, E^{clust} is the energy of the cluster, and η is taken to be η^{track} if the track contains at least four hits in the silicon layers of the ID and η^{clust} otherwise.

Muon candidates are formed by matching reconstructed tracks in the inner detector with either complete or partial tracks reconstructed in the muon spectrometer [13], with the requirement that they satisfy $p_{\text{T}} > 10$ GeV and $|\eta| < 2.4$.

When defining validation regions and control regions containing leptons, in order to measure SM backgrounds, a tighter selection is applied to the selected leptons. For muons, it is required that $\sum p_{\text{T}}$(tracks) in a cone of radius[2] $\Delta R < 0.2$ around the muon must be less than 1.8 GeV (excluding the muon track), while for electrons $\sum p_{\text{T}}$(tracks) in the equivalent cone must be less than 10% of the electron's p_{T}, and the electron must satisfy tighter shower-shape and track requirements [12].

The measurement of the missing transverse momentum two-vector $\vec{p}_{\text{T}}^{\,\text{miss}}$ and its magnitude $E_{\text{T}}^{\text{miss}}$ is then based on the transverse momenta of all electron candidates, all muon candidates (including those which fail the isolation requirement), all jet candidates with $p_{\text{T}} > 7$ GeV and $|\eta| < 4.5$ which are not also electron candidates, and all clusters of calorimeter cells with $|\eta| < 4.5$ not associated to such objects [14].

When candidates passing the object selection overlap with each other, a classification is required to remove all but one of the overlapping objects. Overlaps are resolved based on the distance parameter ΔR based on previous studies [15]. The criteria are applied in the following order: First, if an electron candidate and a jet candidate are found within $\Delta R < 0.2$, the object is interpreted as an electron and the overlapping jet candidate is ignored. Next, if a muon and a jet candidate are found within $\Delta R < 0.4$, the object is treated as a jet and the muon is ignored. Finally, if an electron candidate and a jet candidate are found within $0.2 \leq \Delta R < 0.4$, the object is interpreted as a jet and the nearby electron is ignored.

[2] $\Delta R = \sqrt{(\Delta\eta)^2 + (\Delta\phi)^2}$

Signal region	**7j55**	**8j55**	**9j55**	**6j80**	**7j80**	**8j80**
Number of isolated leptons (e, μ)	$= 0$					
Jet p_{T}	> 55 GeV			> 80 GeV		
Jet $\lvert\eta\rvert$	< 2.8					
Number of jets	≥ 7	≥ 8	≥ 9	≥ 6	≥ 7	≥ 8
$E_{\mathrm{T}}^{\mathrm{miss}} / \sqrt{H_{\mathrm{T}}}$	> 4 GeV$^{1/2}$					

Table 1: Definitions of the six signal regions.

4 Event selection

Following the object reconstruction described in Section 3, events are discarded if they contain any jet failing quality criteria designed to suppress detector noise and non-collision backgrounds, or if they lack a reconstructed primary vertex with five or more associated tracks.

For events containing no isolated electrons or muons, six signal regions (SRs) are defined as shown in Table 1. The first three require at least seven, eight, or nine jets, with $p_{\mathrm{T}} > 55$ GeV; the latter three require at least six, seven, or eight jets, with $p_{\mathrm{T}} > 80$ GeV. The selections are non-exclusive, so events with the largest jet multiplicities can be found in more than one signal region.

The final selection variable is $E_{\mathrm{T}}^{\mathrm{miss}} / \sqrt{H_{\mathrm{T}}}$, the ratio of the magnitude of the missing transverse momentum to the square root of the scalar sum H_{T} of the transverse momenta of all jets with $p_{\mathrm{T}} > 40$ GeV and $|\eta| < 2.8$. This ratio is closely related to the significance of the missing transverse momentum relative to the resolution due to stochastic variations in the measured jet energies [14]. The value of $E_{\mathrm{T}}^{\mathrm{miss}} / \sqrt{H_{\mathrm{T}}}$ is required to be larger than 4 GeV$^{1/2}$ for all signal regions.

The dominant backgrounds are multi-jet production, including purely strong interaction processes and fully-hadronic decays of $t\bar{t}$; semi- and fully-leptonic decays of $t\bar{t}$; and leptonically decaying W or Z bosons produced in association with jets. Non-fully-hadronic $t\bar{t}$, and W and Z are collectively referred to as 'leptonic' backgrounds. Contributions from gauge boson pair and single top quark production are negligible. The determination of the multi-jet and 'leptonic' backgrounds is described in Sections 6 and 7, respectively.

5 Monte Carlo simulations

Monte Carlo simulations are used as part of the 'leptonic' background determination process, and to assess sensitivity to specific SUSY signal models. The 'leptonic' backgrounds are generated using `Sherpa1.4.0` [16] with the `CT10` parton distribution function (PDF) set [17]. For $t\bar{t}$, events are generated with up to four additional partons in the matrix element. W + jets and Z + jets are generated with up to five additional partons in the matrix element. In all cases, additional jets are generated via parton showering together with fragmentation and hadronization. The W + jets, Z + jets and $t\bar{t}$ backgrounds are normalized according to their inclusive theoretical cross sections [18]. In the case of $t\bar{t}$ production, the relative weight of gluon-gluon initiated events to other processes is determined from the goodness of fit to data in the validation regions. The estimation of the 'leptonic' backgrounds in the signal regions is described in detail in Section 7.

Supersymmetric production processes are generated using `Herwig++2.5.2` [19]. Signal cross sections are calculated to next-to-leading order in the strong coupling constant α_S, including the resum-

mation of soft gluon emission at next-to-leading-logarithmic accuracy (NLO+NLL) [20].[3] An envelope of cross-section predictions is defined using the 68% confidence-level (CL) ranges of the `CTEQ6.6` [21] (including the α_S uncertainty) and `MSTW2008 NLO` [22] PDF sets, together with independent variations of the factorization and renormalization scales by factors of two or one half. The nominal cross-section value is then taken to be the midpoint of the envelope, and the uncertainty assigned is half the full width of the envelope, following closely the PDF4LHC recommendations [23]. For illustrative purposes, plots of kinematic quantities show the distribution expected for an example supersymmetric model point with gluino mass of 900 GeV and neutralino mass of 150 GeV, values not excluded in Ref. [5].

6 Multi-jet backgrounds

The dominant background at intermediate values of $E_{\mathrm{T}}^{\mathrm{miss}}$ is multi-jet production including purely strong interaction processes and fully hadronic decays of $t\bar{t}$.[4] These processes are not reliably predicted with existing Monte Carlo calculations, so their contributions must be determined from collision data. The selection cuts have been designed such that multi-jet processes can be determined reliably from supporting measurements.

In events dominated by jet activity, including hadronic decays of top quarks and gauge bosons, the $E_{\mathrm{T}}^{\mathrm{miss}}$ resolution is then approximately proportional to $\sqrt{H_{\mathrm{T}}}$, and is almost independent of the jet multiplicity. The distribution of the ratio $E_{\mathrm{T}}^{\mathrm{miss}}/\sqrt{H_{\mathrm{T}}}$ has a shape that is almost invariant under changes in the jet multiplicity, as shown in Figure 1.[5] The predictions of the multi-jet background in the signal region can then be obtained using the $E_{\mathrm{T}}^{\mathrm{miss}}/\sqrt{H_{\mathrm{T}}}$ distribution with lower jet multiplicity as a template. The templates are then normalised to the selection with the signal region multiplicity in the region $E_{\mathrm{T}}^{\mathrm{miss}}/\sqrt{H_{\mathrm{T}}} < 1.5$. For example, to obtain the multi-jet prediction for the 8j55 signal region, a template describing the shape of the $E_{\mathrm{T}}^{\mathrm{miss}}/\sqrt{H_{\mathrm{T}}}$ distribution is obtained from those events that contain exactly six jets, using the same 55 GeV p_{T} threshold as the target signal region. The six-jet $E_{\mathrm{T}}^{\mathrm{miss}}/\sqrt{H_{\mathrm{T}}}$ template is normalized to the number of eight-jet events observed in the region $E_{\mathrm{T}}^{\mathrm{miss}}/\sqrt{H_{\mathrm{T}}} < 1.5$ GeV$^{1/2}$ after subtraction of the 'leptonic' background expectation. The normalized template then provides a prediction for the multi-jet background for the 8j55 signal region for which $E_{\mathrm{T}}^{\mathrm{miss}}/\sqrt{H_{\mathrm{T}}} > 4$ GeV$^{1/2}$.

For the three signal regions which use a 55 GeV jet p_{T} threshold (7j55, 8j55 and 9j55), the template is obtained using events with exactly six jets above the same 55 GeV threshold. The signal regions with the 80 GeV threshold (6j80, 7j80 and 8j80) all use a template based on events with exactly five jets with the same 80 GeV threshold.

While finite jet resolution leads to $E_{\mathrm{T}}^{\mathrm{miss}}/\sqrt{H_{\mathrm{T}}}$ distributions which are, to a good approximation, invariant under changes in jet multiplicity, ≈35% variations in the shape are observed in validation regions with intermediate values of $E_{\mathrm{T}}^{\mathrm{miss}}/\sqrt{H_{\mathrm{T}}}$ between 1.5 GeV$^{1/2}$ and 3.5 GeV$^{1/2}$. The leading source of this variation is a contribution to $E_{\mathrm{T}}^{\mathrm{miss}}$ from soft calorimeter energy deposits, not associated to jets, and hence not contributing to H_{T}. The effect of these soft energy terms is corrected for by reweighting the $E_{\mathrm{T}}^{\mathrm{miss}}/\sqrt{H_{\mathrm{T}}}$ distribution separately for each jet multiplicity, to provide the same $\sum \mathrm{E}_{\mathrm{T}}^{\mathrm{CellOut}}/H_{\mathrm{T}}$ distribution as each signal region, where $\sum \mathrm{E}_{\mathrm{T}}^{\mathrm{CellOut}}$ is the scalar sum of $E \sin\theta$ over all clusters of calorimeter cells not associated with jets having $p_{\mathrm{T}} > 7$ GeV or electron, or muon candidates. It is these reweighted distributions that are shown in the figures.

Systematic uncertainties on the multi-jet prediction are determined from: the closure of the method

[3] The NLL correction is used for when the gluino mass lies between 200 GeV and 2 TeV. For masses outside this range cross sections at NLO accuracy obtained with `Prospino2.1` [20] are used.

[4] Contributions from hadronic decays of W and Z bosons produced in assiation with jets are also included, but are negligible by comparison.

[5] Compared to Ref. [5], the distribution is narrower, since an improved calibration scheme with better resolution is now used for the jet reconstruction. The better resolution leads to an improved discrimination of signal and background.

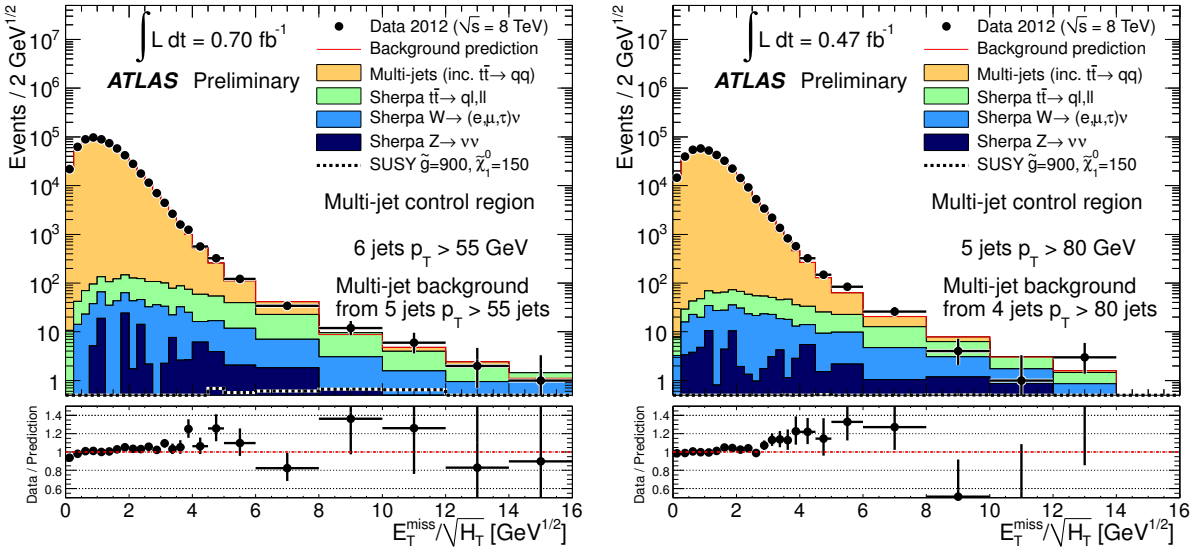

(a) **(b)**

Figure 1: $E_{\mathrm{T}}^{\mathrm{miss}}/\sqrt{H_{\mathrm{T}}}$ distributions in example multi-jet control regions. **(a)** For exactly six jets with $p_{\mathrm{T}} > 55$ GeV, compared to a prediction based on the $E_{\mathrm{T}}^{\mathrm{miss}}/\sqrt{H_{\mathrm{T}}}$ distribution for exactly five jets with $p_{\mathrm{T}} > 55$ GeV. **(b)** For exactly five jets with $p_{\mathrm{T}} > 80$ GeV, compared to a prediction based on four jets with $p_{\mathrm{T}} > 80$ GeV. The multi-jet predictions have been normalized to the data in the region $E_{\mathrm{T}}^{\mathrm{miss}}/\sqrt{H_{\mathrm{T}}} < 1.5$ GeV$^{1/2}$ after subtraction of the predicted 'leptonic' backgrounds. The most important 'leptonic' backgrounds are also shown, based on MC simulations. The contamination of the control region by the example SUSY signal point is consistently small (and always less than 0.5/2 GeV$^{1/2}$ in Fig. b). The error bars on the data points show the Poisson coverage interval corresponding to the number of data events observed in each bin. The integrated luminosity for these lower jet multiplicities is smaller than 5.8 fb^{-1} since the templates and data make use of 'prescaled' triggers; these select events with lower jet multiplicities, but accept only a fraction of the events satisfying that selection.

	$t\bar{t}$ + jets and W + jets		Z + jets
Lepton type	electron	muon	muon
Lepton p_{T}	$p_{\mathrm{T}} > 25$ GeV, $\lvert\eta\rvert < 2.4$		
Lepton $\lvert\eta\rvert$	< 2.47	< 2.4	< 2.4
Lepton multiplicity	$= 1$		$= 2$
m_{T} or $m_{\mu\mu}$	60 GeV $< m_{\mathrm{T}} <$ 100 GeV	40 GeV $< m_{\mathrm{T}} <$ 100 GeV	80 GeV $< m_{\mu\mu} <$ 100 GeV
VR $\rightarrow$ CR transform	$e \rightarrow$ jet	$\mu \rightarrow$ jet	$\mu \rightarrow \nu$
Jet p_{T}, $\lvert\eta\rvert$, mult. (CR)	As in Table 1.		
$E_{\mathrm{T}}^{\mathrm{miss}} / \sqrt{H_{\mathrm{T}}}$ (CR)			

Table 2: Definitions of the validation regions and control regions for the 'leptonic' backgrounds: $t\bar{t}$ + jets and W + jets combined, and Z + jets. The validation regions VR are defined by the first five selection requirements. The control regions CR differ from the VR in their treatment of the charged leptons, and by having additional requirements on jets and $E_{\mathrm{T}}^{\mathrm{miss}} / \sqrt{H_{\mathrm{T}}}$, as shown in the final two rows.

(10 − 25%), heavy-quark fraction (10 − 25%), calibration of non-associated clusters (up to 10%), and 'leptonic' background subtraction (10 − 15%), in each case closely following the methods of Ref. [5].

7 'Leptonic' backgrounds

Non-fully-hadronic (i.e. semi-leptonic or di-leptonic) $t\bar{t}$, and W and Z production are collectively referred to as 'leptonic' backgrounds. The process $Z \rightarrow \nu\nu$ + jets contributes to the signal regions since it produces jets in association with $E_{\mathrm{T}}^{\mathrm{miss}}$. Leptonic $t\bar{t}$ and W decays contribute to the signal regions when hadronic τ decays allow them to evade the lepton veto, with smaller contributions from events in which electrons or muons are produced but are not reconstructed.

The 'leptonic' background predictions employ the Monte Carlo simulations described in Section 5. When predictions are taken directly from the Monte Carlo, the 'leptonic' background event yields are subject to uncertainties of typically 40% from the use of a leading-order Monte Carlo generator and experimental uncertainties from Monte Carlo modelling of: the jet energy scale (JES, 30 − 55%), the jet energy resolution (JER, 5%), the number of multiple proton-proton interactions (6%), the lepton trigger and reconstruction efficiency and the lepton momentum scale. The numbers in parentheses indicate the typical values of the SR event yield uncertainties in the raw MC prediction. The uncertainty in the integrated luminosity is 3.6%.

To reduce uncertainties from higher-order corrections and from Monte Carlo modelling and detector response, background predictions are, where possible, normalized to data using control regions (CR) and cross-checked against data in other validation regions (VR). These control regions and validation regions are designed to be distinct from, but kinematically close to, the signal regions. The use of control regions is effective in reducing uncertainties from Monte Carlo modelling and detector response. For example the typical uncertainty in the event yield resulting from higher-order QCD correction is reduced from 40% to 8% and that from the jet energy scale from 50% to 5%.

The control and validation regions are defined as shown in Table 2. By using control regions that are kinematically similar to the signal regions, experimental and theoretical uncertainties, including those arising from the use of a leading-order generator, are reduced.

The $t\bar{t}$ + jets and W + jets validation regions require a single electron or muon. Kinematic distributions, including the jet multiplicity distribution, show good agreement between data and Monte Carlo.

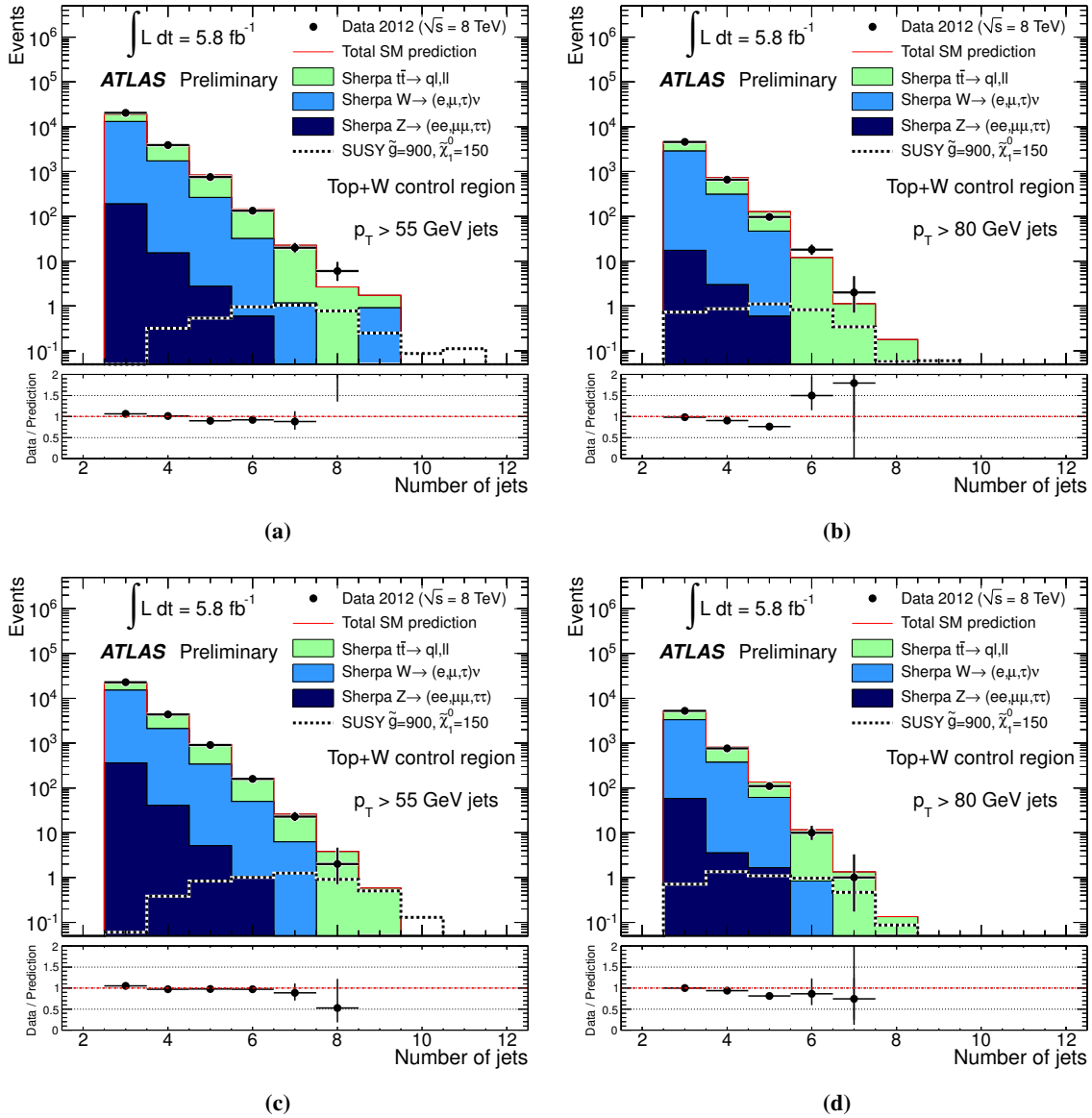

Figure 2: Distributions of jet multiplicities in the control regions with exactly one electron (top) or exactly one muon (bottom), for jet p_{T} threshold of 55 GeV (left) and 80 GeV (right).

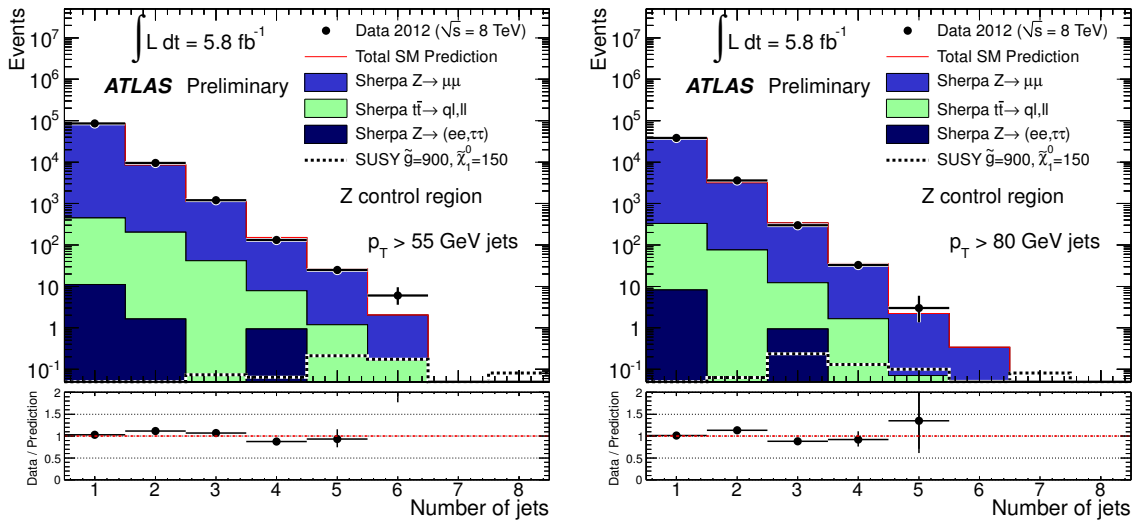

Figure 3: The jet multiplicity distributions for two different jet p_{T} cuts for the $Z \to \mu\mu$ + jets control region selection.

Since it is dominantly through hadronic τ decays that W and $t\bar{t}$ contribute to the signal regions, the corresponding control regions are created by recasting the muon or electron as a jet (Figure 2). The additional jet may, if it has sufficient p_{T}, contribute to H_{T}, and hence to the selection variable $E_{\mathrm{T}}^{\mathrm{miss}}/\sqrt{H_{\mathrm{T}}}$.

The Monte Carlo prediction for $Z \to \nu\nu$ in association with jets is checked using an enhanced $Z \to \mu\mu$ + jets distribution, obtained by selecting events with precisely two isolated muons (and no isolated electrons) with di-muon invariant mass consistent with the mass of the Z boson. The related control regions are formed from these validation regions by recasting the muons as neutrinos, and then recalculating $E_{\mathrm{T}}^{\mathrm{miss}}$ (Figure 3).

As described in Ref. [5], for each control region in which the Monte Carlo simulations predict at least one event for 5.8 fb^{-1}, the 'leptonic' background prediction in the corresponding signal region is determined by scaling the Monte Carlo event prediction by the transfer factor that would correctly normalize MC to data in the control region.

8 Results, interpretation and limits

Figure 4 shows the $E_{\mathrm{T}}^{\mathrm{miss}}/\sqrt{H_{\mathrm{T}}}$ distributions after applying the jet selections for the six different signal regions (see Table 1 for their definitions) prior to the final $E_{\mathrm{T}}^{\mathrm{miss}}/\sqrt{H_{\mathrm{T}}} > 4$ GeV$^{1/2}$ requirement. Figure 5 shows the jet multiplicity distributions for the two different jet p_{T} thresholds after the final $E_{\mathrm{T}}^{\mathrm{miss}}/\sqrt{H_{\mathrm{T}}}$ requirement. It should be noted that the jet multiplicity selection is non-exclusive, so the same events can contribute to multiple signal regions. The 'leptonic' backgrounds shown in the figures are those calculated from the Monte Carlo simulation, using the MC calculation of the cross section and normalized to 5.8 fb^{-1}.

The number of events observed in each of the six signal regions, as well as their Standard Model background expectations are shown in Table 3. Good agreement is observed between SM expectations and the data for all six signal regions. Table 3 also shows the 95% confidence-level upper bound $N_{\mathrm{BSM,max}}^{95\%}$ on the number of events originating from sources other than the Standard Model, and the corresponding upper limit $\sigma_{\mathrm{BSM,max}}^{95\%} \times A \times \epsilon$ on the cross section times efficiency within acceptance (which equals the

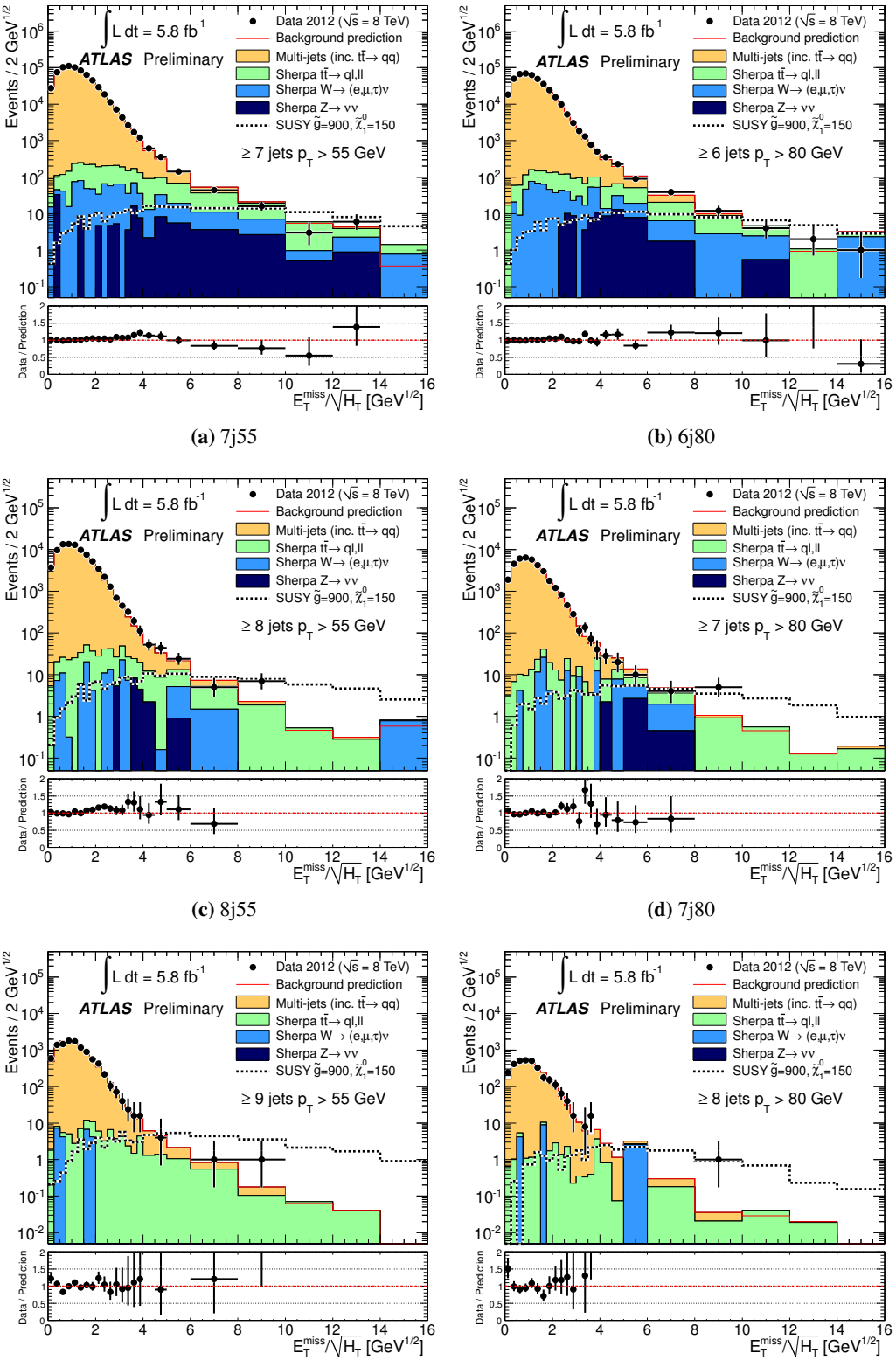

(a) 7j55 **(b)** 6j80

(c) 8j55 **(d)** 7j80

(e) 9j55 **(f)** 8j80

Figure 4: The distribution of the variable $E_{\mathrm{T}}^{\mathrm{miss}}/\sqrt{H_T}$ for each of the six different signal regions defined in Table 1, prior to the final $E_{\mathrm{T}}^{\mathrm{miss}}/\sqrt{H_{\mathrm{T}}} > 4$ GeV$^{1/2}$ requirement.

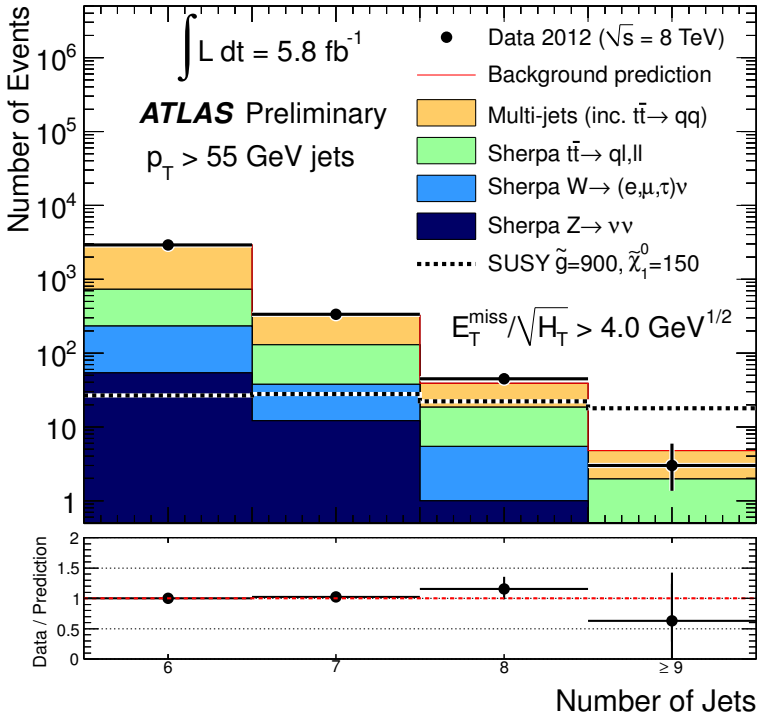

(a)

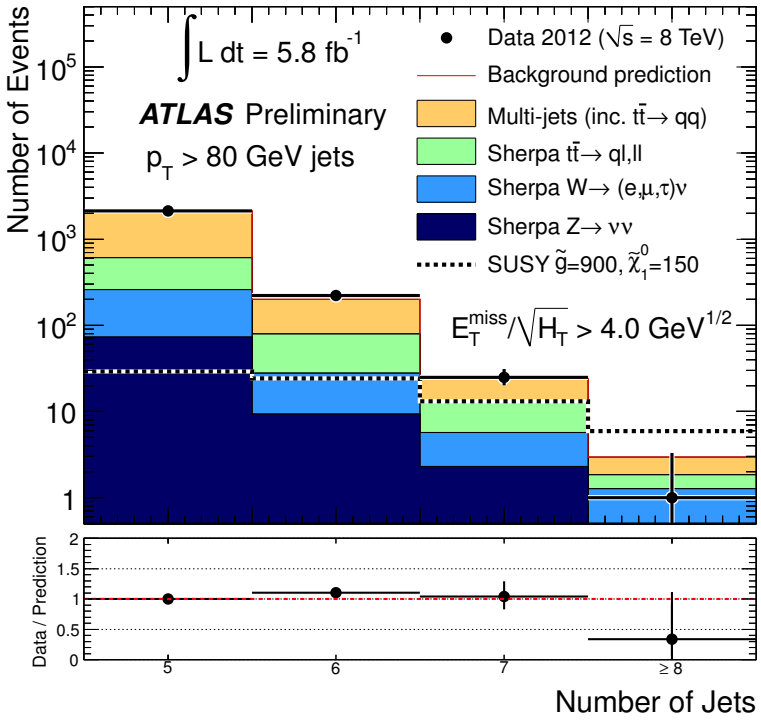

(b)

Figure 5: The distribution of jet multiplicity for jets with $p_{\mathrm{T}} > 55$ GeV **(a)** and those with $p_{\mathrm{T}} > 80$ GeV **(b)**. Only events with $E_{\mathrm{T}}^{\mathrm{miss}} / \sqrt{H_{\mathrm{T}}} > 4$ GeV$^{1/2}$ are shown.

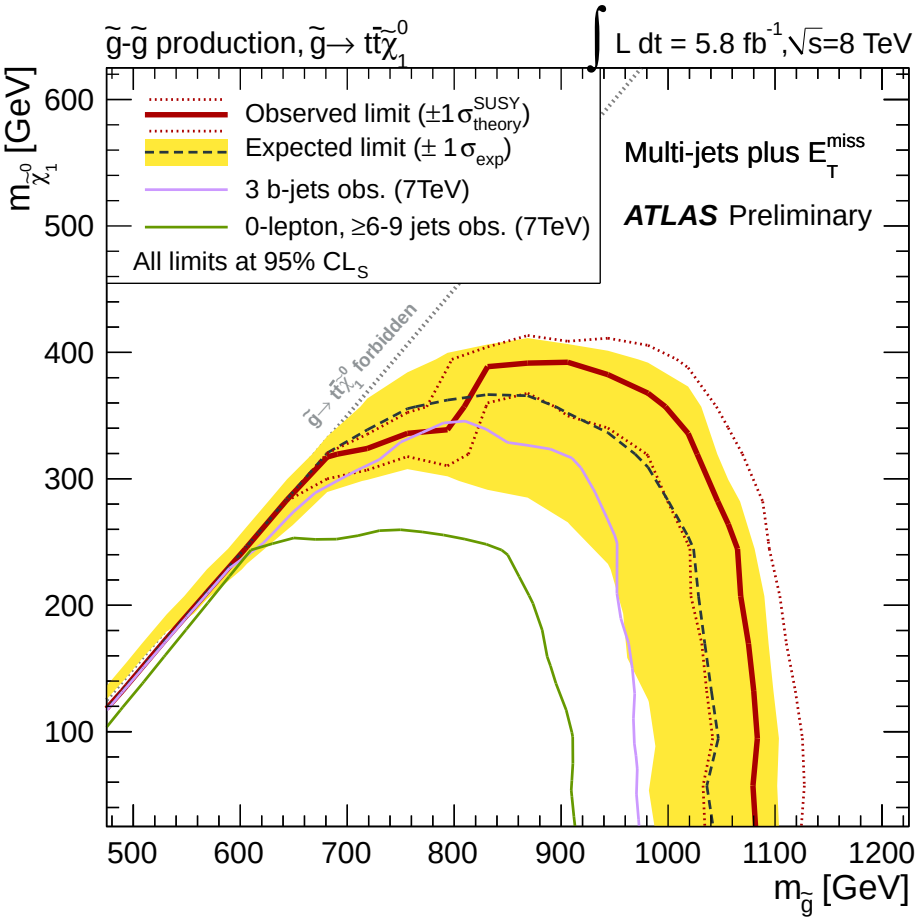

Figure 6: Combined 95% CL exclusion curve for the simplified gluino-neutralino model. The dashed grey and solid red lines show the 95% CL expected and observed limits, respectively, including all uncertainties except the theoretical signal cross section uncertainty (PDF and scale). The shaded yellow band around the expected limit shows the $\pm1\sigma$ result. The $\pm1\sigma$ lines around the observed limit represent the result produced when moving the signal cross section by $\pm1\sigma$ (as defined by the PDF and scale uncertainties). The observed limits are also shown for a 3 b-jet + $E_{\mathrm{T}}^{\mathrm{miss}}$ search [6] and from the 7 TeV multi-jet + $E_{\mathrm{T}}^{\mathrm{miss}}$ analysis [5].

Signal region	**7j55**	**8j55**	**9j55**	**6j80**	**7j80**	**8j80**
Multi-jets	219 ± 39	23 ± 7	2.8 ± 0.9	134 ± 32	12 ± 4	1.1 ± 0.4
$t\bar{t} \to q\ell, \ell\ell$ and $W(\to \ell\nu)$ + jets	121^{+23}_{-25}	18 ± 8	$2.0^{+2.2}_{-1.3}$	97 ± 24	14^{+10}_{-12}	$1.8^{+1.7}_{-1.4}$
$Z(\to \nu\nu)$ + jets	13 ± 13	1 ± 1	$0^{+0.4}$	12 ± 12	2 ± 2	$0^{+0.4}$
Total Standard Model	353 ± 48	42 ± 10	$4.8^{+2.4}_{-1.6}$	243 ± 42	28^{+11}_{-12}	$2.9^{+1.8}_{-1.5}$
Data	381	48	3	248	26	1
$N^{95\%}_{\mathrm{BSM,max}}$ (exp)	101	24	7.3	88	26	5.5
$N^{95\%}_{\mathrm{BSM,max}}$ (obs)	122	29	5.4	91	25	4
$\sigma^{95\%}_{\mathrm{BSM,max}} \cdot A \cdot \epsilon$ (exp) [fb]	17.5	4.1	1.3	15.2	4.5	0.9
$\sigma^{95\%}_{\mathrm{BSM,max}} \cdot A \cdot \epsilon$ (obs) [fb]	21	5	0.9	15.7	4.3	0.7

Table 3: Results for each of the six signal regions for an integrated luminosity of $5.8\,\mathrm{fb}^{-1}$. The expected numbers of Standard Model events are given for each of the following sources: multi-jet (including fully-hadronic $t\bar{t}$), semi- and fully-leptonic $t\bar{t}$ decays combined, and W and Z bosons (separately) in association with jets, as well as the total Standard Model expectation. The uncertainties on the predictions show the combination of the statistical and systematic components. Where small event counts in control regions have not made it possible to determine a central value for the expectation, an asymmetric bound is given instead. The numbers of observed events are also shown. The final five rows show the statistical quantities described in the text. Both the expected (exp) and the observed (obs) values are shown for $N^{95\%}_{\mathrm{BSM,max}}$ and $\sigma^{95\%}_{\mathrm{BSM,max}} \times A \times \epsilon$.

limit on the observed number of signal events divided by the luminosity).

In the absence of significant discrepancies, limits are set in the context of a simplified supersymmetric model, containing only a gluino octet and a neutralino $\tilde{\chi}^0_1$ within kinematic reach, and decaying with unit probability according to Eq. 1. Theoretical uncertainties on the SUSY signals are estimated as described in Section 5. Combined experimental systematic uncertainties on the signal yield from jet energy scale, resolution, and data quality requirements are approximately $15 - 25\%$.

The limit for each signal region is obtained by comparing the observed event count with that expected from Standard Model background plus SUSY signal processes, taking into account all uncertainties on the Standard Model expectation, including those which are correlated between signal and background (for instance jet energy scale uncertainties) and all but theoretical cross section uncertainties (PDF and scale) on the signal expectation. The resulting exclusion regions, shown in Figure 6, are obtained using the CL_s prescription [24], taking the signal region with the best expected limit at each point in parameter space. The position of the 95% CL exclusion bound is determined by the 9j55 signal region for large $m(\tilde{g})$ and small $m(\tilde{\chi}^0_1)$, and by the 8j55 signal region at larger $\tilde{\chi}^0_1$ mass where the three-body decay process $\tilde{g} \to t + \bar{t} + \tilde{\chi}^0_1$ is close to its kinematic limit. The product of the signal acceptance and the efficiency close to the 95% CL exclusion bound is in the range 1%–20% depending on the signal region. Within the context of the simplified model, the 95% CL exclusion boundLimits on sparticle masses quoted in the text are those from the lower edge of the $1\,\sigma$ signal cross section band rather than the central value of the observed limit, so can be considered conservative. on the gluino mass is 1.0 TeV for lightest neutralino masses up to 300 GeV.

9 Summary

A search for new physics is presented using final states containing large jet multiplicities in association with missing transverse momentum. The search uses a sample of the 2012 pp LHC data taken at $\sqrt{s}$ = 8 TeV, collected with the ATLAS detector, and corresponding to an integrated luminosity of 5.8 fb^{-1}. For a gluino mass around 1 TeV the increase in centre-of-mass energy from 7 TeV to 8 TeV leads to an enhancement in the gluino-gluino cross section by a factor of about 2.4.

Six non-exclusive signal regions are defined. The first three require at least seven, eight or nine jets, with $p_{\mathrm{T}} > 55$ GeV; the latter three require at least six, seven or eight jets, with $p_{\mathrm{T}} > 80$ GeV. In all cases the events are required to satisfy $E_{\mathrm{T}}^{\mathrm{miss}} / \sqrt{H_{\mathrm{T}}} > 4$ GeV$^{1/2}$, and to contain no isolated high-p_{T} electrons or muons.

In each of the six signal regions, agreement is found between the Standard Model prediction and the data. In the absence of significant discrepancies, the results significantly extend the constraints on any models predicting large numbers of jets in association with an invisible particle or particles, including R-parity conserving supersymmetry models. An example interpretation is shown in the context of a simplified R-parity conserving supersymmetry model, in which both of the pair-produced gluinos decay via the process $\tilde{g} \rightarrow t + \bar{t} + \tilde{\chi}_1^0$. Within this simplified model, gluinos with masses smaller than about 1.0 TeV are excluded at the 95% confidence level for $\tilde{\chi}_1^0$ masses up to 300 GeV.

References

[1] H. Miyazawa, *Baryon number changing currents*, Prog. Theor. Phys. **36 (6)** (1966) 1266–1276.

P. Ramond, *Dual theory for free fermions*, Phys.Rev. **D3** (1971) 2415–2418.

Y. Golfand and E. Likhtman, *Extension of the algebra of Poincaré group generators and violation of p invariance*, JETP Lett. **13** (1971) 323–326.

A. Neveu and J. Schwarz, *Factorizable dual model of pions*, Nucl.Phys. **B31** (1971) 86–112.

A. Neveu and J. Schwarz, *Quark model of dual pions*, Phys.Rev. **D4** (1971) 1109–1111.

J.-L. Gervais and B. Sakita, *Field theory interpretation of supergauges in dual models*, Nucl.Phys. **B34** (1971) 632–639.

D. Volkov and V. Akulov, *Is the neutrino a Goldstone particle?*, Phys.Lett. **B46** (1973) 109–110.

J. Wess and B. Zumino, *A Lagrangian model invariant under supergauge transformations*, Phys.Lett. **B49** (1974) 52.

J. Wess and B. Zumino, *Supergauge transformations in four dimensions*, Nucl.Phys. **B70** (1974) 39–50.

P. Fayet, *Supersymmetry and weak, electromagnetic and strong interactions*, Phys.Lett. **B64** (1976) 159.

P. Fayet, *Spontaneously broken supersymmetric theories of weak, electromagnetic and strong interactions*, Phys.Lett. **B69** (1977) 489.

G. R. Farrar and P. Fayet, *Phenomenology of the production, decay, and detection of new hadronic states associated with supersymmetry*, Phys.Lett. **B76** (1978) 575–579.

P. Fayet, *Relations between the masses of the superpartners of leptons and quarks, the Goldstino couplings and the neutral currents*, Phys.Lett. **B84** (1979) 416.

S. Dimopoulos and H. Georgi, *Softly broken supersymmetry and SU(5)*, Nucl.Phys. **B193** (1981) 150.

[2] H. Goldberg, *Constraint on the photino mass from cosmology*, Phys.Rev.Lett. **50** (1983) 1419.

J. R. Ellis, J. Hagelin, D. V. Nanopoulos, K. A. Olive, and M. Srednicki, *Supersymmetric relics from the big bang*, Nucl.Phys. **B238** (1984) 453–476.

[3] ATLAS Collaboration, *The ATLAS experiment at the CERN Large Hadron Collider*, JINST **3** (2008) S08003.

[4] ATLAS Collaboration, *Search for new phenomena in final states with large jet multiplicities and missing transverse momentum using $\sqrt{s}$ = 7 TeV pp collisions with the ATLAS detector*, JHEP **11** (2011) 099, arXiv:1110.2299 [hep-ex].

[5] ATLAS Collaboration, *Hunt for new phenomena using large jet multiplicities and missing transverse momentum with ATLAS in 4.7 fb^{-1} of $\sqrt{s}$ = 7 TeV proton-proton collisions*, arXiv:1206.1760 [hep-ex].

[6] ATLAS Collaboration, *Search for top and bottom squarks from gluino pair production in final states with missing transverse energy and at least three b-jets with the ATLAS detector*, arXiv:1207.4686 [hep-ex].

[7] ATLAS Collaboration, *Luminosity determination in pp collisions at $\sqrt{s}$ = 7 TeV using the ATLAS detector in 2011*, . ATLAS-CONF-2011-116.

[8] M. Cacciari, G. P. Salam, and G. Soyez, *The anti-k_t jet clustering algorithm*, JHEP **04** (2008) 063, arXiv:0802.1189.

[9] M. Cacciari and G. P. Salam, *Dispelling the N^3 myth for the k_t jet-finder*, Phys. Lett. **B641** (2006) 57–61, arXiv:hep-ph/0512210.

[10] C. Issever, K. Borras, and D. Wegener, *An improved weighting algorithm to achieve software compensation in a fine grained LAr calorimeter*, Nucl.Instrum.Meth. **A545** (2005) 803–812, arXiv:physics/0408129 [physics].

[11] ATLAS Collaboration, *Jet energy measurement with the ATLAS detector in proton-proton collisions at sqrt(s) = 7 TeV*, arXiv:1112.6426 [hep-ex].

[12] ATLAS Collaboration, *Search for supersymmetry in final states with jets, missing transverse momentum and one isolated lepton in $\sqrt{s}$ = 7 TeV pp collisions using 1 fb^{-1} of ATLAS data*, Phys. Rev. **D85** (2012) 012006, arXiv:1109.6606 [hep-ex].

[13] ATLAS Collaboration, *Determination of the muon reconstruction efficiency in ATLAS at the Z resonance in proton-proton collisons at $\sqrt{s}$ = 7 TeV*, ATLAS-CONF-2011-008, Feb, 2011.

[14] ATLAS Collaboration, *Performance of Missing Transverse Momentum Reconstruction in Proton-Proton Collisions at 7 TeV with ATLAS*, Eur.Phys.J. **C72** (2012) 1844, arXiv:1108.5602 [hep-ex].

[15] ATLAS Collaboration, *Expected performance of the ATLAS experiment - detector, trigger and physics*, CERN-OPEN-2008-020. arXiv:0901.0512.

[16] F. Krauss, R. Kuhn, and G. Soff, *AMEGIC++ 1.0: A Matrix element generator in C++*, JHEP **0202** (2002) 044, arXiv:hep-ph/0109036 [hep-ph].

T. Gleisberg and S. Hoeche, *Comix, a new matrix element generator*, JHEP **12** (2008) 039, arXiv:0808.3674.

[17] H.-L. Lai, M. Guzzi, J. Huston, Z. Li, P. M. Nadolsky, et al., *New parton distributions for collider physics*, Phys.Rev. **D82** (2010) 074024, arXiv:1007.2241 [hep-ph].

[18] M. Aliev, H. Lacker, U. Langenfeld, S. Moch, P. Uwer, et al., *HATHOR: HAdronic Top and Heavy quarks crOss section calculatoR*, Comput. Phys. Commun. **182** (2011) 1034–1046, arXiv:1007.1327 [hep-ph].

K. Melnikov and F. Petriello, *Electroweak gauge boson production at hadron colliders through $O(\alpha_s^2)$*, Phys. Rev. **D74** (2006) 114017, arXiv:hep-ph/0609070.

[19] M. Bahr et al., *Herwig++ physics and manual*, Eur. Phys. J. **C58** (2008) 639–707, arXiv:0803.0883.

[20] W. Beenakker, R. Hopker, M. Spira, and P. M. Zerwas, *Squark and gluino production at hadron colliders*, Nucl. Phys. **B492** (1997) 51–103, arXiv:hep-ph/9610490.

A. Kulesza and L. Motyka, *Threshold resummation for squark-antisquark and gluino-pair production at the LHC*, Phys.Rev.Lett. **102** (2009) 111802, arXiv:0807.2405 [hep-ph].

A. Kulesza and L. Motyka, *Soft gluon resummation for the production of gluino-gluino and squark-antisquark pairs at the LHC*, Phys.Rev. **D80** (2009) 095004, arXiv:0905.4749 [hep-ph].

W. Beenakker, S. Brensing, M. Kramer, A. Kulesza, E. Laenen, et al., *Soft-gluon resummation for squark and gluino hadroproduction*, JHEP **0912** (2009) 041, arXiv:0909.4418 [hep-ph].

W. Beenakker, S. Brensing, M. Kramer, A. Kulesza, E. Laenen, et al., *Squark and gluino hadroproduction*, Int.J.Mod.Phys. **A26** (2011) 2637–2664, arXiv:1105.1110 [hep-ph].

[21] P. M. Nadolsky et al., *Implications of CTEQ global analysis for collider observables*, Phys. Rev. **D78** (2008) 013004, arXiv:0802.0007.

[22] A. Martin, W. Stirling, R. Thorne, and G. Watt, *Parton distributions for the LHC*, Eur.Phys.J. **C63** (2009) 189–285, arXiv:0901.0002 [hep-ph].

[23] M. Botje, J. Butterworth, A. Cooper-Sarkar, A. de Roeck, J. Feltesse, et al., *The PDF4LHC Working Group Interim Recommendations*, arXiv:1101.0538 [hep-ph].

[24] A. Read, *Presentation of search results: the CL_s technique*, Journal of Physics G: Nucl. Part. Phys. **28** (2002) 2693–2704.